Journal of Materials Chemistry C

ROYAL SOCIETY OF CHEMISTRY

PAPER

View Article Online
View Journal | View Issue

Cite this: *J. Mater. Chem. C*, 2025, **13**, 21040

Luminescent lanthanide coordination polymers for the detection of nitro explosives and efficient identification of latent fingerprints

Nitin Shukla, Juhi Sayala, Goutam Panigrahi and Ashis K. Patra *

The uniquely rich photophysical properties of luminescent lanthanide probes and their complementary favorable ionic interactions with hard nitro groups in nitroaromatic compounds (NACs) make them highly desirable optical probes for the detection of dangerous nitroaromatic explosives and the detection and visualization of latent fingerprints (LFPs). We present two new coordination polymers (**CPs**) utilizing a bottom-up approach: $[Eu_2(ctpy)_6{\cdot}3H_2O]_n$ (**Eu-CP**) and $[Tb_2(ctpy)_6{\cdot}3H_2O]_n$ (**Tb-CP**) (Hctpy = 4′-carboxy-4,2′:6′,4′-terpyridine). The molecular structures of both CPs were systematically analyzed using a range of solid- and solution-based material characterization techniques. The **Eu-CP** and **Tb-CP** displayed bright red and green emissions, respectively, attributed to the $^5D_J \rightarrow {}^7F_J$ f–f transitions from Eu(III) and Tb(III) upon photo-excitation with UV light *via* ctpy as the antenna. The **Eu-CP** probe can be used to detect nitro explosives in the solution and vapor phases by employing turn-off luminescence in the presence of 2,4,6-trinitrotoluene (TNT). Through several spectroscopic studies and observations, a plausible mechanism of interaction was established, wherein the TNT molecules quench the potential PeT-mediated energy transfer (EnT) pathway from ctpy to Eu(III). The results demonstrate that the **Eu-CP** exhibits high selectivity and sensitivity, with an LOD of 18 ppm. **Eu-CP**-impregnated solid-state films can be washed to remove TNT and reused for up to 8 times, demonstrating the practical applicability of the recyclable solid-state film-based sensors. Additionally, the intense red emissions allowed the use of the **Eu-CP** as phosphor powder for the sensitive detection, development, and effective visualization of latent fingerprints (LFPs) demonstrating its practical applicability in forensic science. The **Eu-CP** phosphor powder offers permanent and direct colorful visualization of LFPs with minimal background interference and allows improved detection and capture of fingerprints on various surfaces compared to the existing cumbersome approaches. Notably, the **Eu-CP** exhibits exceptional sensitivity and can detect aged fingerprints with up to level-3 high-resolution traits. The **Eu-CP** phosphor powder was tested using dusting for the development of aged and charged fingerprints on various surfaces for practical use in forensic science. The **Eu-CP** could be suitable for developing reliable fingerprint databases, quickly comparing individuals with hallmark differentiation and deriving deep insights utilizing big data analytics-based artificial intelligence (AI) for bio-authentication and forensic applications.

Received 12th June 2025,
Accepted 23rd August 2025

DOI: 10.1039/d5tc02283e

rsc.li/materials-c

Introduction

Lanthanides have garnered significant attention across various interdisciplinary modern research areas due to their intriguing and unique optical, magnetic, and catalytic properties. Recently, there has been considerable interest in creating well-defined crystalline materials that have adaptable and controllable structural topologies along with high thermodynamic stability for use in optical sensors, LEDs, lasers, biomedicine, imaging, forensic sciences, storage, separation, catalysis, *etc.*[1–7] These emissive lanthanide materials offer superior optical features such as narrow f–f emission bands, large pseudo Stokes shifts, wide luminescence window (UV-Vis-NIR), and long luminescence lifetimes (μs–ms), which make them ideal for targeted luminescent sensing. Their advantages over organic chromophores include reduced photobleaching, reusability, rapid response time, and compatibility with time-resolved detection for background-free signal collection.[8–15] Furthermore, supramolecular probes (*e.g.*, CPs and MOFs) allow increased receptor–analyte interactions through the pores/vacant binding sites, miniaturization of sensors, ease of handling, long-term stability, and reusability, which have driven researchers to focus on building Ln(III)-based solid

Department of Chemistry, Indian Institute of Technology Kanpur, Kanpur 208016, Uttar Pradesh, India. E-mail: akpatra@iitk.ac.in

luminescent sensors. Efficient detection relies primarily on complementary electronic and structural interactions between the sensor and chemical analyte. Nitroaromatic compounds (NACs), as high-energy materials (HEM), are utilized as explosives in mining, solid-state fuels (propellants), and in military applications for national defense; thus, these compounds represent a global security risk and present environmental concerns. Therefore, rapid and selective detection of nitro-rich compounds/explosives (*e.g.*, TNT, RDX, and PETN) is crucial for the prevention of terrorism and for homeland security.[16–21] Traditional methods of detection of NACs are based on calorimetric sensor arrays, GC-MS, and ion mobility spectrometry (IMS), *etc.*, which are often time-consuming, cumbersome, and expensive. This has prompted the exploration of luminescence probes as promising alternatives owing to their high sensitivity, rapid response and easy usability.[22–28] Fluorescent functional materials, such as metal–organic frameworks (MOFs) and coordination polymers (CPs), have shown significant potential for selective explosive detection and have been reviewed.[20,21,29–33] Lanthanide-based materials, due to the oxophilic nature of trivalent Ln(III) ions and their strong affinity for nitro groups *via* HSAB-type electrostatic interactions, enable highly selective and sensitive detection.[3] The Huang group reported a series of mixed lanthanide (Eu/Tb, Eu/Gd, Tb/Gd and Eu/Tb/Gd) coordination polymers (CP) as ratiometric sensors of picric acid[34a] and Eu-CPs as sensors for nitro-rich compounds/explosives.[34b,c] Mahata *et al.* reported Eu-doped-Y-MOF as an efficient turn-off sensor for nitro explosives.[35] The Mandal group reported a Tb(III) sensor based on mixed poly pyridyl-carboxylate and utilized it for the detection of various NACs.[18] Ning *et al.* also reported a Tb(III)-CP for highly sensitive detection of 4-nitrophenol using TRL measurements.[36] Das and coworkers reported the use of 2D nanosheets with (Eu/Tb)-CP for the detection of FOX-7, a new generation of explosive.[37] The Romero group reported Eu(III)-picolinate-based CPs as highly selective turn-off sensors for nitroaromatic compounds (NACs).[38]

The unique, sharp, line-like, distinct luminescence features of Ln(III) ions are not easily replicated and thus can serve as effective optical anticounterfeiting measures in various high-quality products, crucial authentic documents, security, forensics, and biometric authentication database management systems.[39–42] A range of industries have invested in creating optical anticounterfeiting technologies to authenticate and preserve governmental archives such as expensive brand items, bank notes, educational/financial/legal/registry documents, high-value foods, pharmaceuticals, and works of art. Fingerprint detection and development are one of the common counterfeiting measures applied for identification, database management, and crime scene investigations. These have also found importance in banking, authentication (security papers, bonds, *etc.*), and access to personal devices (mobile, laptops, *etc.*). While several latent fingerprint development techniques are discussed in the cited reviews (*e.g.*, cyanoacrylate fuming method, ninhydrin method, vacuum metal deposition, and fluorescent dye staining), we have focused on the powder-dusting methodology using coordination polymers due to its direct relevance to our synthesized material and its alignment with previously reported MMD-based approaches.[39,43,44] The selection of appropriate techniques depends on the specific type of fingerprint and often involves limitations such as potential damage to fingerprints, age, missed traits, operator hazards, and substrate color selectivity. Hence, the development of a universal method to effectively visualize and enhance different types of latent fingerprints would significantly enhance the convenience and efficiency of collecting evidence at the crime scene and facilitate database management.[39,43,44] The bright luminescence, precise emission bands, photobleaching resistance, long luminescence lifetime, large pseudo-Stokes shift and emission in the visible region from Eu(III) and Tb(III) make them ideal luminescent phosphor materials for the effective detection and development of LFP.[39–41,43,44] Commonly, Eu(III) and Tb(III) phosphors, emitting in the red or green regions, are used for easy visualization and direct image capture and analysis under UV light, offering permanence without photobleaching. Notably, the Wang group reported a MOF membrane as a fluorescent material for detecting visible fingerprints.[45] Later, the Li group also reported an Eu-MOF for the detection of nitro explosives and fingerprint development.[46] Ning *et al.* also reported an Eu(III) coordination polymer to detect LFPs on various surfaces.[47] Lei Jia's group reported a stimuli-responsive fluorescent material doped with Eu(III) and Tb(III) for application in latent fingerprint identification.[48] Lesniewski *et al.* reported a new strategy, wherein *in situ* interaction with the Eu(III) complex was used to visualize latent fingermarks.[49] Saif's group also reported a Eu(III) nanophosphor-based strategy for use as an anticounterfeiting measure and for the detection of latent fingerprints.[50]

Luminescent Ln-coordination polymers (Ln-CPs) are ideal platforms for NAC sensing due to the oxophilicity of Ln(III) ions and the electron-deficient nature of NACs, which facilitate strong ionic interactions and PET-driven luminescence quenching through donor–acceptor mechanisms. In this work, we have designed two chemically and thermodynamically stable Ln(III)-coordination polymers: $[Eu_2(ctpy)_6{\cdot}3H_2O]_n$ (**Eu-CP**) and $[Tb_2(ctpy)_6{\cdot}3H_2O]_n$ (**Tb-CP**) using 4′-carboxy-4,2′:6′,4′-terpyridine (Hctpy) as bridging antennae (Scheme 1). The coordination polymers were structurally characterized using SC-XRD, PXRD and FT-IR analyses. Furthermore, structurally similar **La-CP** was utilized as a diamagnetic analog to study the solution-state speciation using NMR spectroscopy. The strongly emissive **Eu-CP** was used to rapidly detect nitro explosives, more specifically TNT, in solution as well as in the solid state using time-resolved luminescence (TRL) with high sensitivity (LOD = 18 ppm). The **Eu-CP** was found to exhibit reversible non-covalent binding with TNT and was reusable up to 8 times upon washing. Additionally, the latent fingerprints (LFP) were captured and developed using the intense red emission from the luminous **Eu-CP** phosphor powders. The material could be used to detect and develop LFPs on a variety of surfaces with a high degree of precision and level-3 characteristic trait qualities. The powdered **Eu-CP** with multiple Eu(III) centers enhances the luminescence intensity and photostability for prolonged LFP analysis in forensic studies. Moreover, the easily

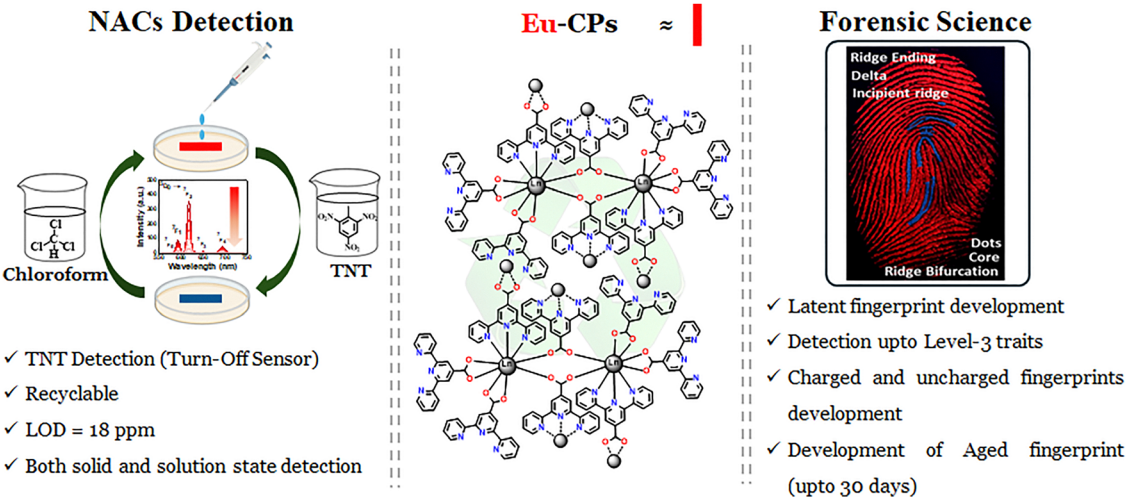

Scheme 1 Schematic of the **Eu/Tb-CP**s studied in this work and the two targeted applications using these CPs: nitro-aromatic compound (NAC)–based explosive detection (left) and latent fingerprint (LFP) development (right) using the responsive luminescence features of **Eu/Tb-CPs**.

grounded microcrystalline solid-state powder form makes this material ideal for solvent-free dusting-based fingerprint development, unlike many soluble Eu(III) complexes that often require matrix embedding and thereby risk smearing or signal loss. The **Eu-CP** is also promising for clear detection and visualization of aged and charged fingerprints according to forensic guidelines, leveraging the uniquely appropriate optical features of the f–f transitions from **Eu-CP** (Scheme 1).

Results and discussion

Design aspects

The antenna, 4′-carboxy-4,2′:6′,4′-terpyridine (Hctpy), served the dual purpose of enabling efficient energy transfer to the emissive Ln(III) ion and providing multiple binding sites (*i.e.*, N_3 (tpy) and CO_2^-) around Ln(III). Moreover, the hard CO_2^- acts as a bridging moiety, thereby enabling the formation of multimetallic systems as coordination polymers (**CP**) as **Eu-CP** and **Tb-CP**. The strongly chelating Hctpy ligand, containing N_3-donor terpyridine and CO_2^- as hard bases in the Ln(III) binding pockets, provides coordinative saturation and high thermodynamic stability to the CPs. The strong red and green luminescence in the visible region, originating from f → f transitions, is achieved by maximizing the ET to the Ln(III) due to the presence of three ctpy antennae around Eu(III) or Tb(III) ions. These attributes permit the use of the highly luminescent coordination polymers as solid-state luminescent sensors for hard oxyanions, and can potentially allow them to be used as emissive phosphors for the latent fingerprint (LFP) detection and development by the powder dispersion method.

Synthesis and characterization

The Hctpy antenna was prepared using a slight modification of a reported procedure.[51] We subjected 2-acetyl pyridine to aldol condensation with furan-2-carboxaldehyde in the presence of 2 equiv. of NaOH. The addition of excess ammonia (25%) formed 4′-(furan-2-yl)-2,2′:6′,2″-terpyridine (ftpy/[**1**]), which, on further oxidation with aq. $KMnO_4$, yielded 4′-carboxy-4,2′:6′,4′-terpyridine (Hctpy) ligand as an off-white solid in 40% yield (the synthetic scheme is shown in Fig. S1, SI). The ftpy intermediate and Hctpy ligand were characterized using ^1H and ^{13}C NMR spectroscopy, ESI-MS and FT-IR spectroscopy (Fig. S2–S4, SI). The Eu(III) and Tb(III) coordination polymers (*i.e.*, **Eu-CP** and **Tb-CP**) were prepared by solvothermal synthesis using the base-pretreated Hctpy solution with the respective lanthanide triflate salts in 3 : 1 mole ratio in water, in a sealed

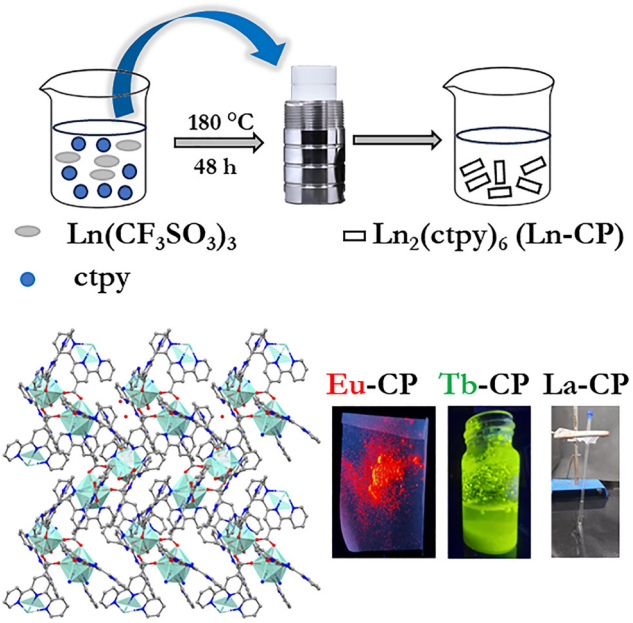

Fig. 1 General solvothermal synthetic route for the preparation of Ln(III)-coordination polymers (Ln-CPs). The synthesis involved heating $Ln(CF_3SO_3)_3$ and Hctpy as a 1 : 3 mixture at 180 °C for 48 h. The polycrystalline powders showed red (**Eu-CP**) and green (**Tb-CP**) luminescence when placed under a 365 nm UV lamp.

Teflon-lined stainless-steel autoclave at 180 °C for 48 h (Fig. 1).[52] Transparent crystals were obtained upon cooling to room temperature at a rate of 20 °C h^{-1}. The molecular structures of the coordination polymers (Ln-CPs) were determined using single-crystal X-ray diffraction analysis and named as **Eu-CP** and **Tb-CP**. The structurally similar **La-CP**, as a diamagnetic non-emissive analogue, was also synthesized using a similar procedure to gain insight into the molecular structures and interactions of the **Ln-CPs** with the studied analytes. Details of the synthesis procedure and characterizations of the Ln-CPs are given in the experimental section.

Crystal structure

The crystal structures of Eu and Tb-coordination polymers (**Eu-CP** and **Tb-CP**) are shown in Fig. 2, 3 and Fig. S5 (SI), and a representative Chemdraw depiction is given in Fig S6 (SI). The **Eu-CP** and **Tb-CP** crystallize in the monoclinic $P2_{1/n}$ space group. The generalized molecular formula based on the repeating unit for the coordination polymer is $[Ln_2(ctpy)_6{\cdot}3H_2O]_n$, labeled as Ln-CPs [Ln = Eu(III) for **Eu-CP**, Tb(III) for **Tb-CP**]. The X-ray structures reveal the presence of two Ln(III) centers bridged by $-COO^-$ groups in μ-η^1:η^1-coordination mode from the two antennas (ctpy), and their N_3-donor sites are coordinated to other Ln(III) ions in the crystal lattice of the CPs. Additionally, the carboxylate (CO_2^-) moieties from two other ctpy ligands coordinated to Ln(III) in a η^2-chelating mode. One ctpy ligand bound through the N_3-donor site of the tpy end to each Ln(III), and the η^2-CO_2^- end to the other Ln(III) in the CP. Thus, overall, each Ln(III) has a nine-coordinated $\{LnN_3O_6\}$ monocapped square-antiprism geometry (Fig. 2b). The tripositive charge of Ln(III) is balanced by two η^2-CO_2^- and two bridging μ-η^1:η^1-COO^- groups. The Eu–Eu internuclear distance is 5.132(3) Å in **Eu-CP**, while the Tb–Tb distance is 5.168(4) Å in **Tb-CP**. The Eu–O (η^2-CO_2^-) bond lengths range from 2.415(2) Å to 2.553(3) Å in **Eu-CP**, while the Tb–O (η^2-CO_2^-) bond lengths range from 2.385(3) Å to 2.532(3) Å in **Tb-CP**. For bridging μ-η^1:η^1-COO^- bonds, the Eu–O bond length spans from 2.329(3) Å to 2.422(2) Å, and Tb–O bond ranges from 2.390(3) Å to 2.532(3) Å. The Ln-N bond distance with the neutral tpy donor ranges from 2.539(3) Å to 2.664(3) Å for **Eu-CP** and 2.518(3) Å to 2.640(3) Å for **Tb-CP**. The subtle differences in Ln–O *vs.* Ln–N bond lengths in the CPs are presumably due to the greater ionic character of Ln^{3+}–O(CO_2^-) bonds compared to neutral Ln–N (tpy) bonds in these CPs. Additionally, three co-crystallized water molecules in the unit cell further stabilize these systems through intermolecular hydrogen bonding. The cell packing parameters are listed in Table S1 (SI). The powdered crystalline sample of **Eu-CP** was subjected to powder-XRD to study the bulk purity of the phosphor powder material used for the detection and development of latent fingerprints. The **Eu-CP** shows sharp, intense diffraction peaks from the crystalline planes. The experimental diffraction pattern matches well with the simulated pattern obtained from the SC-XRD data, suggesting a long-range bulk purity of the coordination

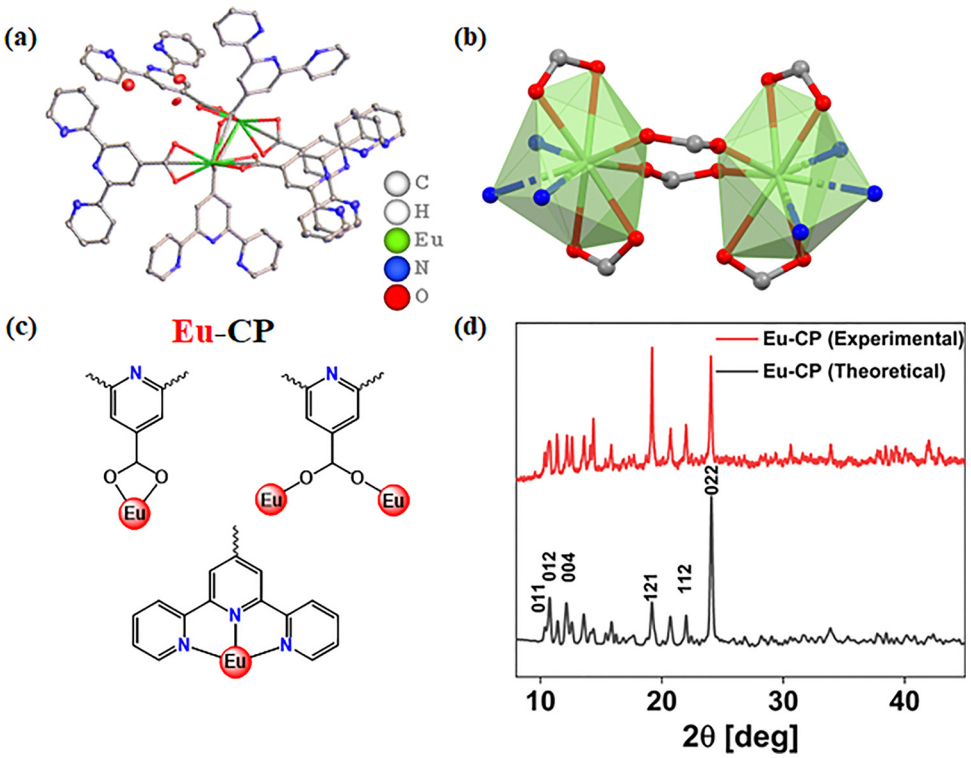

Fig. 2 Structural and photophysical characterization of $[Eu_2(ctpy)_6]_n$ **(Eu-CP)**. (a) Asymmetric unit of the **Eu-CP** crystal. (b) Coordination environment and geometry around the Eu(III) center. (c) Binding mode of ctpy moiety to the Eu(III) ion in the crystal lattice. (d) PXRD pattern of the polycrystalline powder in comparison to the simulated PXRD spectra.

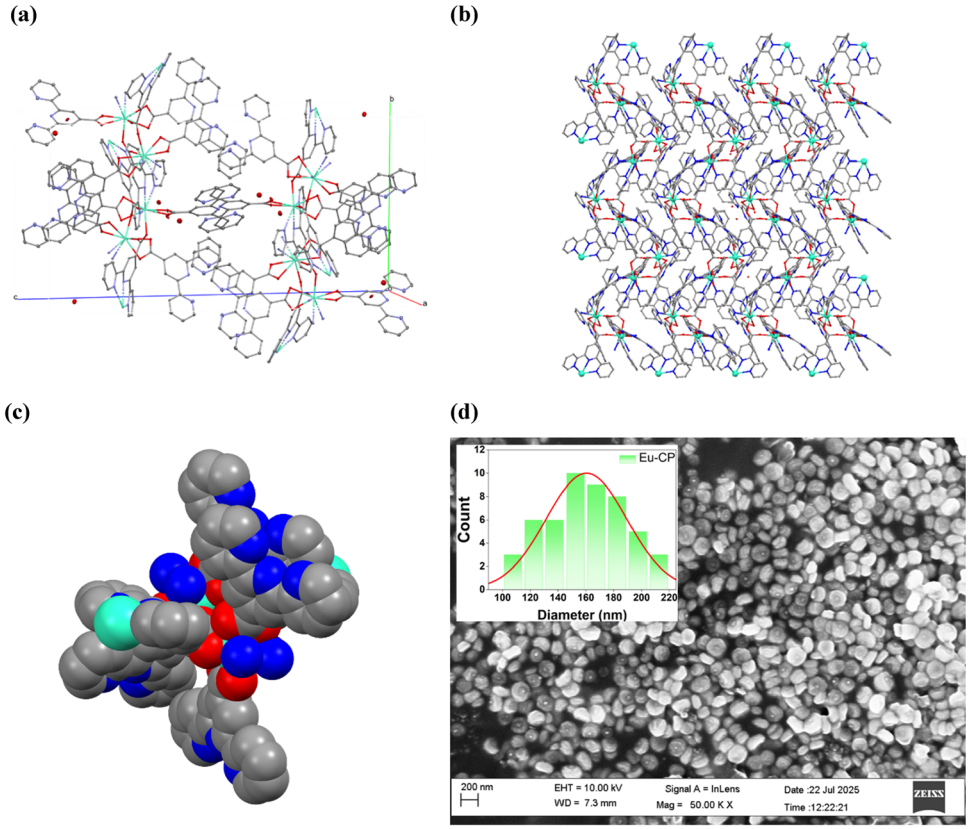

Fig. 3 Molecular structure of **Eu-CP** representing (a) the unit cell packing for the **Eu-CP**, showing the coordination environment around the Eu(III) and (b) the three-dimensional view of the crystal packing of the **Eu-CP**. **(c)** Space-filled model of the **Eu-CP** showing that the central Eu(III) ions are completely protected and buried by the antennae, thereby providing additional stability against external analytes. (d) FESEM images of the powdered sample of the **Eu-CP** showing particles with sizes in the nanometer range. Inset: Size distribution histogram diagram for particles calculated (d_{av} ~ 160 nm) from the FE-SEM image using ImageJ software.

polymers. Some characteristic planes with maximum intensity are labeled in Fig. 2(d). A representative view of the coordination polymer, its unit cell packing and a space-filled model are also provided, which advocates for the rigidity and stability of the **Eu-CP** (Fig. 3(a)–(c)). We also performed scanning electron microscopy (SEM) on the powdered sample to determine the size of the particles and their morphology. As shown in Fig. 3(d), the particles are uniformly distributed, with a predominantly spherical morphology and an average particle size of ~160 nm, as determined from the analysis of over 50 particles using ImageJ image analysis software. The relatively small and uniform particle size is advantageous for strong surface adhesion to latent fingerprint residues, while the spherical morphology promotes even dispersion and consistent coverage, which are critical for high-resolution fingerprint visualization.

To understand the solution-state speciation and interactions with the analyte, we prepared a structurally similar diamagnetic lanthanum-based coordination polymer (**La-CP**). The ^{1}H NMR spectrum of **La-CP** exhibits all the ctpy ligand-based peaks with a slight chemical shift, suggesting the formation, stability and structural integrity of the Ln-CPs in the solution state (Fig. S7 and S8, SI). **La-CP** was later used for ^{1}H and ^{13}C NMR studies in solution, allowing analysis of the corresponding adduct structures with NACs through NMR titration studies for mechanistic investigation.

Photophysical studies

The synthesized coordination polymers exhibit poor solubility and remain insoluble in most common organic solvents. Therefore, all the solution state studies were performed with a freshly prepared suspended sample (1.5 mg in 30 mL CH_3CN), which was subjected to sonication for 30 min and then left undisturbed for 24 h. A 200 μL aliquot was then taken in 1800 μL of solvent (CH_3CN) for UV-Vis, fluorescence, and NMR characterization, and various spectroscopic titration studies.

UV-Vis spectroscopy

The Hctpy antenna exhibits a sharp absorption maximum at ~280 nm (ε = 42 000 M^{-1} cm^{-1}), characteristic of $\pi \rightarrow \pi^*$ transitions in the highly conjugated terpyridine system, along with a weaker peak at ~320 nm (ε = 20 600 M^{-1} cm^{-1}), possibly due to $n \rightarrow \pi^*$ transitions from the electron-rich N and O centers. The suspended supernatant from the sonicated CPs also shows a similar absorption profile. The CPs exhibit a λ_{max} of ~279 nm (**Eu-CP**, **Tb-CP**), with a shoulder at ~316 nm (**Eu-CP**) and at 318 nm (**Tb-CP**). The extensive overlap and similarity of the absorption profile of CPs with the free Hctpy ligand support the conclusion that the absorption is solely ligand-based in the coordination polymers. Moreover, the coordination to Eu(III)/

Tb(III) did not apparently affect the absorption profile of the Hctpy antenna, indicative of a minimal role of the shielded 4f orbitals in Ln-ctpy bonding, and its predominantly ionic nature. An overlay of the UV-Vis absorption profiles for Hctpy, **Eu-CP**, and **Tb-CP** is given in Fig. S9 (SI).

Luminescence properties

The photoluminescence spectra for the **Eu-CP** and **Tb-CP** probes were recorded with an Agilent Cary Eclipse spectrophotometer at 298 K using the supernatant from the sonicated coordination polymers. When excited at 328 nm, the time-resolved luminescence spectrum shows all the characteristic traits of the Eu(III) and Tb(III) from the **Eu-CP** and **Tb-CP**, originating from their respective f → f transitions ($^5D_0 \rightarrow {}^7F_J$, J = 0–4 for **Eu-CP** and $^5D_4 \rightarrow {}^7F_J$, J = 6–1 for **Tb-CP**), in all common organic solvents (Fig. S10, SI). The intense red luminescence from **Eu-CP** originated from the $^5D_0 \rightarrow {}^7F_2$ hypersensitive electric dipole (ED)-allowed transition at 615 nm and used as a reliable spectroscopic yardstick for luminescence titrations with NACs. The steady-state emission spectra did not show any apparent bands for the ctpy ligand, suggesting an efficient energy transfer (ET) to Eu(III) and Tb(III). The excitation spectra for **Eu-CP** and **Tb-CP** show two intense bands at ~328 nm and 282 nm, comparable to the Hctpy absorption profile, which indicates effective energy transfer (ET) from the Hctpy antenna. Furthermore, the luminescence decay lifetime of **Eu-CP** for the $^5D_0 \rightarrow {}^7F_2$ transitions (615 nm) was 1.00(±0.020) ms and of **Tb-CP** for the $^5D_4 \rightarrow {}^7F_5$ transitions (545 nm) was 0.74(±0.020) ms at λ_{ex} = 328 nm. The excitation and emission spectra along with excited state lifetime measurements are presented in Fig. S11 (SI). Given the superior optical parameters of **Eu-CP** compared to **Tb-CP**, we focus on the detection of nitro-explosives and latent fingerprint development using **Eu-CP**.

Nitro explosive detection

The luminescence sensing by **Eu-CP** of 2,4,6-trinitrotoluene (TNT), as a typical nitro explosive, and other analogous nitroaromatic compounds was investigated. The time-resolved luminescence profile of **Eu-CP**, originating from the Eu(III) center, was quenched on the addition of nitroaromatic compounds with an additional electron-withdrawing group (–COOH, –CHO, NO_2, *etc.*) at the *ortho*- or *para*-positions. This led us to test the detection of nitro-rich explosives, more precisely TNT, containing three -NO_2 groups. For this purpose, TNT was synthesized *via* nitration of 4-nitrotoulene using

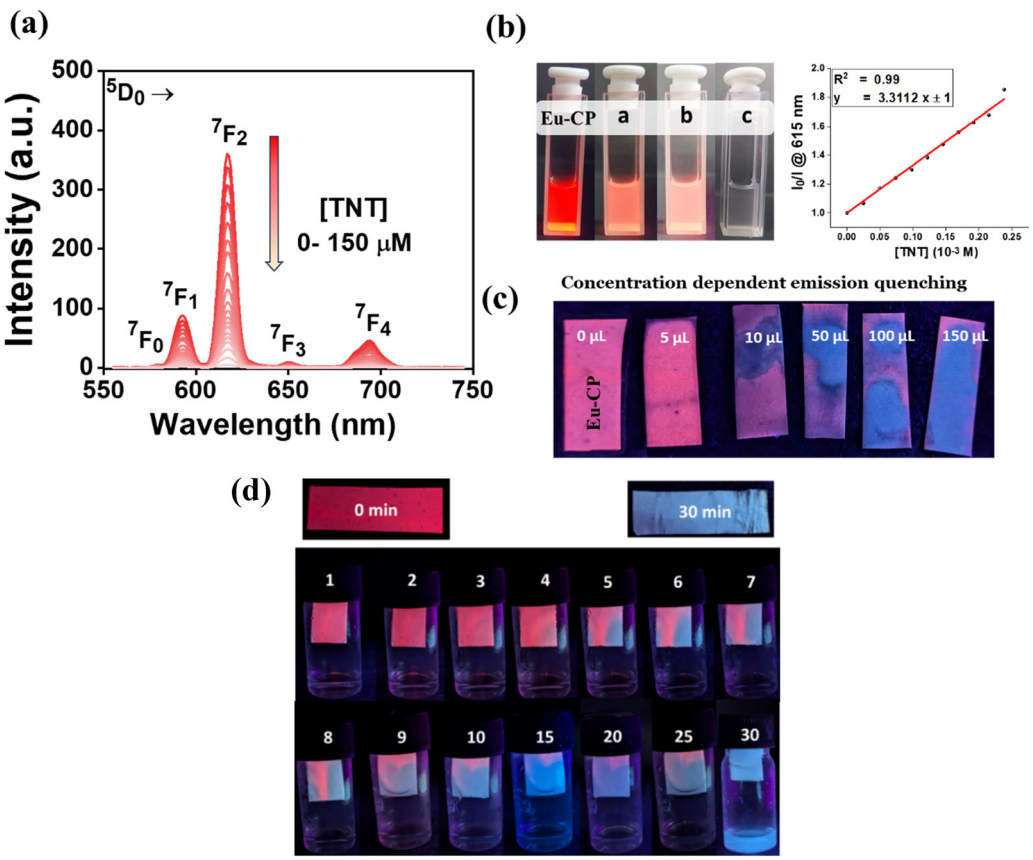

Fig. 4 (a) Emission response of **Eu-CP** dispersed in CH_3CN with continuous addition of TNT and (b-left) their changes as visible under a 365 nm UV lamp. **Eu-CP** dispersed in MeCN (1.5 mg in 15 mL), λ_{ex} = 328 nm, T = 298 K. (b-right) Changes in emission intensity (I_0/I) as produced on the addition of [TNT] for calculation of the Stern–Volmer quenching constant. (c) Luminescent strips were prepared by impregnating **Eu-CP** on Whatman paper upon consecutive addition of TNT (5 mM, CH_3CN) and visualized under 365 nm UV light (concentration test: different volumes of TNT were applied to the strips). (d) Time-dependent vapor phase detection of TNT. **Eu-CP** strips suspended over TNT solution in $CHCl_3$ (0–30 min, 298 K).

fuming nitric acid, and the product was recrystallized and characterized by ^{1}H and ^{13}C NMR spectroscopic analyses.

A 5 mM stock solution of TNT was prepared in acetonitrile, which was added consecutively to **Eu-CP** with simultaneous measurements of absorption and phosphorescence intensities. The absorption spectra show an increase in absorbance around 260 nm that is ascribed to TNT absorption. The time-resolved luminescence intensity was measured concurrently with the successive additions of a 5 mM solution of TNT in acetonitrile. The TRL intensity steadily decreased with increasing concentration of TNT, and was completely quenched upon the addition of ~150 μM of TNT solution (Fig. 4a). No further changes in emission profile or intensity were observed with the addition of up to a 50-fold excess of TNT. Thus, the **Eu-CP** acted as a Turn-OFF luminescent sensor for TNT. To gain more insights into the binding affinity and mechanism of interaction of **Eu-CP** with TNT, the Stern–Volmer quenching constant (K_{SV} = 3.3×10^{3} M^{-1}) was calculated from the luminescence titration (Fig. 4b), showing a relatively weaker binding affinity with the probe *via* non-covalent interactions and suggesting opportunity for possible reusability. The calculated limit of detection (LOD) of 18 ppm for TNT was remarkable compared to the previously reported probes (S12, SI). The absorption spectra were also monitored with successive addition of TNT, revealing an increase in the intensity at ~260 nm, characteristic of TNT absorption, without the formation of any isosbestic point(s). This indicates that the TNT molecules lead to dynamic quenching and do not perturb the core structures of the coordination polymer (Fig. 4a and Fig. S13, SI).

To probe its design and practical utility in NAC-explosive detection kits, the **Eu-CP** probe was also tested in its impregnated solid-phase form for vapor-phase detection of TNT. The solid-phase detection strips were prepared by impregnating **Eu-CP** on a piece of Whatman paper by simply dipping it into a suspended solution of **Eu-CP**. The air-dried strips showed characteristic bright red luminescence from Eu(III) when illuminated with a 365 nm UV lamp. Adding varying concentrations of TNT to the strip and exposing it to a 365 nm UV lamp produced a similar quenching effect (Fig. 4c). The strips were also suspended above a saturated TNT solution in chloroform, and time-dependent digital images were captured under 365 nm UV light exposure (Fig. 4d). The color of the strip shifted from bright red to blue within 10 min, and became completely blue in about 30 min, indicating gradual quenching of Eu(III) luminescence upon interaction with the TNT vapor. These quenched blue strips were then washed with $CHCl_3$ and dried in an oven, which resulted in a gradual reappearance of the red emission. Up to eight repetitions of the cyclic quenching and recovery of red emission were performed, which demonstrates that the sensor strips are reversible and recyclable (Fig. S14, SI). This observation indicates that the TNT does not alter the coordination environment of **Eu-CP**, and possibly resides and interacts at the surface or in the interstitial sites of the **Eu-CP**. To confirm the hypothesis, we conducted PXRD analysis and NMR titration experiments with the probe and the TNT. PXRD patterns of the **Eu-CP** were recorded before and after the addition of TNT. Although the sharp, intense peaks from different crystal planes decreased, the system did not break into the amorphous state and retained its crystallinity upon interaction with TNT. After washing the TNT-containing powdered sample multiple times with chloroform, the PXRD pattern returned to its original profile (Fig. 5a). The weakly bound TNT is thus released and washed away with chloroform. The same titration experiment was conducted and analyzed by ^{1}H NMR spectroscopy using the structurally similar diamagnetic **La-CP**. Even with a 20-fold excess of TNT, there were no discernible changes in the ^{1}H NMR spectrum of the analogous **La-CP** (Fig. S15, SI). This also implies that the coordination polymer retained its structural integrity, and did not dissociate or change morphology upon interaction with TNT. Additionally, the hydration number (q) was determined from the lifetimes (τ) after the addition of TNT in H_2O and D_2O using

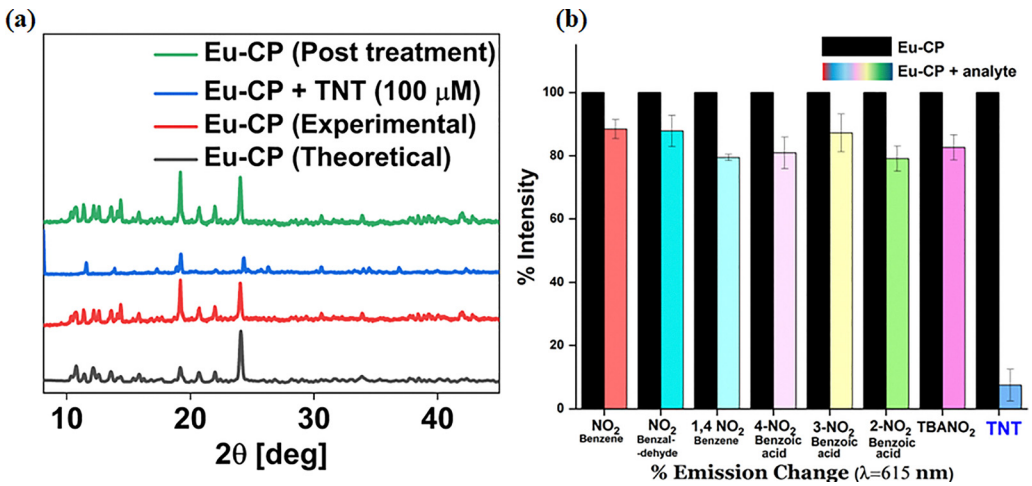

Fig. 5 (a) PXRD patterns of the **Eu-CP** before and after TNT addition and after washing with chloroform. (b) Bar plots showing the selective response produced from the **Eu-CP** (solution state) after the addition of different interferants (nitroaromatic compounds).

Horrocks' equation to identify the possible binding and dissociation of solvent (eqn (1)). The determined q value of approximately 0 for **Eu-CP** suggests there is no accessible coordination site at Eu(III) in the **Eu-CP** coordination polymer for direct interaction with the nitro group of TNT *via* solvent exchange; rather, TNT is bound on the surface or interstitial pockets in CP *via* non-covalent interaction. The **Eu-CP** (solution state) yields a selective response for TNT with the remarkable quenching compared to insignificant TRL-quenching upon the addition of different nitro-aromatic compounds as interferants (*i.e.*, TBA-NO_3, 4-nitrobenzaldehyde, 1,4-dinitrobenzene, 4-nitrobenzoic acid, 3-nitrobenzoic acid, 2-nitrobenzoic acid, *tert*-butyl nitrate) (Fig. 5b and Fig. S16, S17, SI).

Based on the PXRD data of the samples before and after addition to TNT, solution-state photophysical studies, luminescence titrations, Stern–Volmer quenching constants, lifetime and hydration numbers (q), reversibility, and recyclability of the **Eu-CP** impregnated solid-state sensor, we suggest a possible luminescence sensing mechanism of TNT by the **Eu-CP** probe. In the **Eu-CP** probe, upon photo-excitation at λ_{ex} = 328 nm, the efficient energy transfer from the ctpy antenna to the Eu(III) results in strong Eu(III)-based red luminescence, as evident from its dispersed solution and the solid-state paper strips under UV light. However, upon interaction of the TNT with the **Eu-CP** probe in solution or over solid-state paper strips, the TNT molecules were bound on the surface or in the interstitial sites of the **Eu-CP** coordination polymer. The close proximity of TNT and **Eu-CP** facilitates efficient energy transfer from the excited state antenna to the LUMO of the TNT, followed by relaxation *via* photo-induced electron transfer (PeT) to the highly electron-withdrawing nitro groups of TNT. This PeT process thereby prevents ET from the antenna to sensitize Eu(III), resulting in significant quenching of the luminescence intensity of **Eu-CP** upon interaction with TNT. Subsequently, in the solid-state powder or in the impregnated solid-state films, by simple washing of the powdered sample or paper strips with chloroform, the TNT is washed away, and PeT is no longer operative, thereby restoring the original red luminescence the **Eu-CP** probe and allowing its reuse (Fig. 6). The selective luminescence quenching observed for TNT is attributed to its higher electron affinity and favorably positioned excited state energy, which promotes efficient PeT from the excited **Eu-CP** to TNT. Other nitroaromatics such as NB, DNB, and NP have lower electron affinities, resulting in weaker or negligible quenching. Additionally, the substituent positioning on TNT may allow better π–π stacking and interaction with the porous surface of **Eu-CP**, further enhancing its selective sensing.

Detection and development of latent fingerprint (LFP)

Encouraged by the strong luminescence of the **Eu-CP** as phosphor powder, we further extended its application for the effective development and detection of latent fingerprints (LFP). Currently, the multi-metal powder deposition method is widely used; in this approach, metallic compounds are used as phosphor agents for the development of specific fingerprints (Fig. 7a). We utilized **Eu-CP** in the powder deposition method for visualization and analysis of latent fingerprints. The **Eu-CP** offers permanent and direct colorful visualization of LFPs with minimal background interference and the ability to rapidly detect and identify fingerprints at a higher level of sensitivity on a variety of surfaces compared to existing cumbersome approaches.

To begin, the crystalline sample of **Eu-CP** was finely powdered before the development of LFPs. Multiple volunteers were selected to account for multiple types of fingerprints and were asked to deposit their fingerprints on various common surfaces at different times of the day, to account for intra-

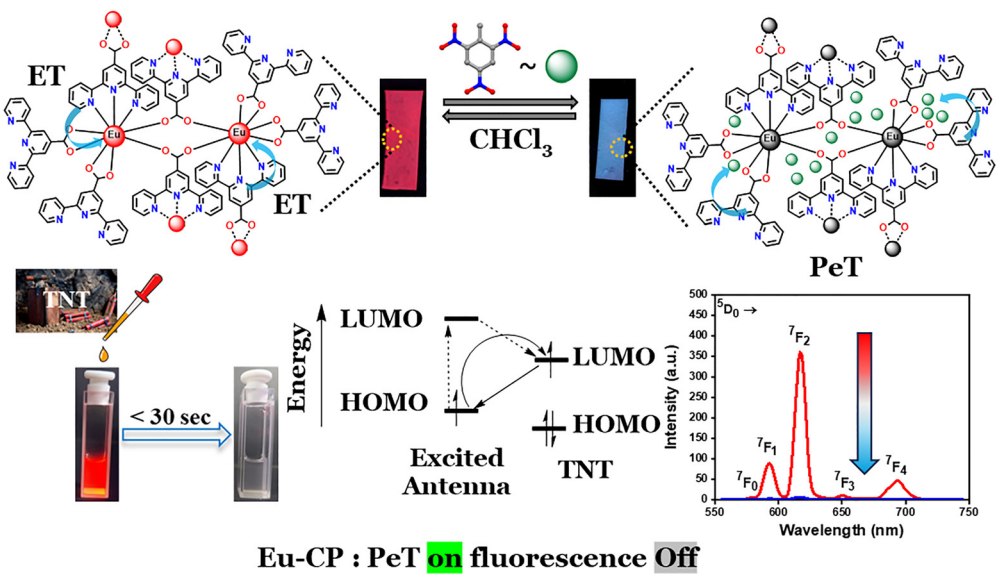

Fig. 6 Probable mechanism for **Eu-CP** emission quenching by TNT. TNT trapped inside the structural interstitial sites facilitates photo-induced electron transfer (PeT) from the excited antenna. This prevents energy transfer and thereby quenching of red emission from **Eu-CP**. Washing with $CHCl_3$ removes TNT from the proximity of the probe, making the strips glow red again.

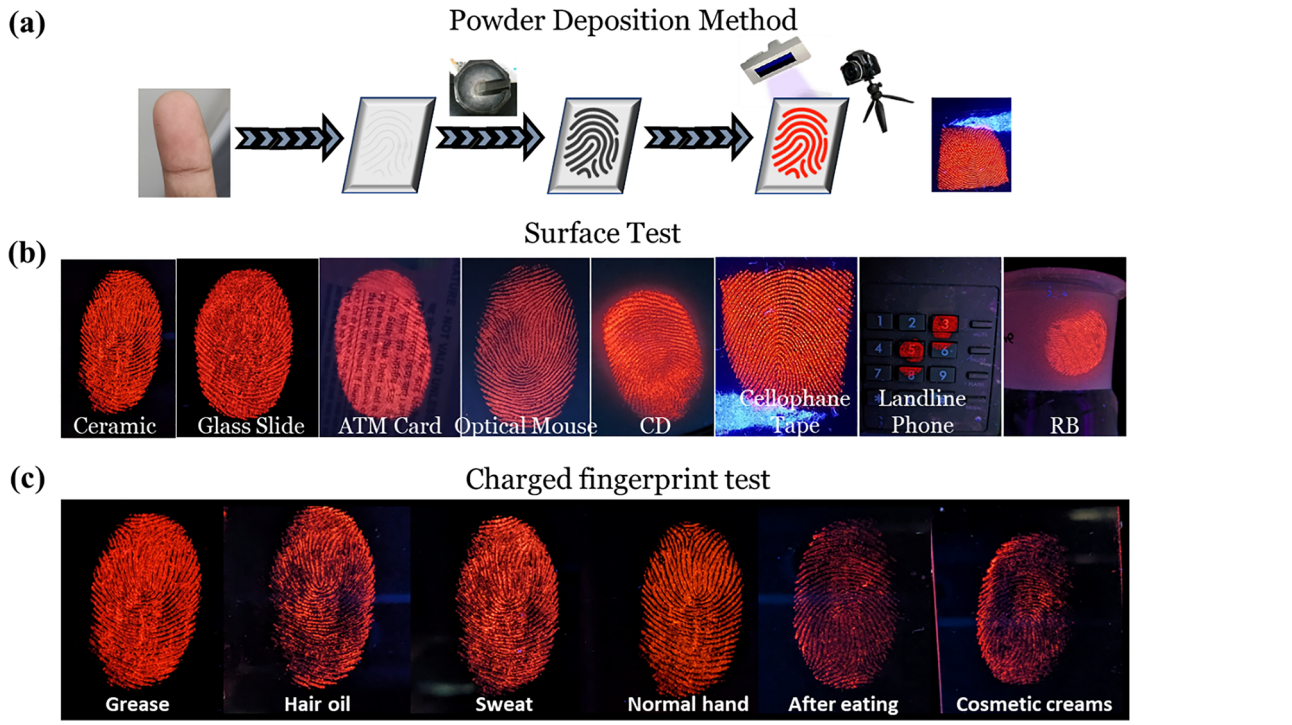

Fig. 7 (a) Schematic of the image development technique used for the detection of latent fingerprints (LFPs). (b) Surface test showing the images of the developed fingerprints on various substrates using the **Eu-CP** under a 365 nm UV lamp. (c) Fingerprint development using charged (grease and oils) fingers. The bright luminescence properties of the **Eu-CP** phosphor powder allow the development of fingerprints on both normal and charged surfaces with visualization of level 1–3 traits.

donor variations, and after different daily activities, to account for charged (oiled) fingerprints. To account for the typical deterioration of LFPs that occurs during forensic investigations, the samples were aged for 24 hours before the development. A finely ground sample of **Eu-CP** was then added and allowed to soak for 15 min. The excess sample was then cleaned up with a fine brush and an air gun. Although the LFPs were invisible to the naked eye, all the identifiable marks and traits were clearly visible after their development using the **Eu-CP**-based phosphor powder with exposure to 365 nm UV light. The emissive images of the developed LFPs were then digitally captured in a dark chamber under 365 nm UV light. The **Eu-CP** phosphor powder was utilized to develop fingerprints created on various commonly encountered surfaces (*viz.* ceramics, a glass slide, an ATM card, an optical mouse, a phone surface, cellophane tape, and a round-bottom flask) to assess its practical applicability (Fig. 7b and Fig. S18–S22, SI). The **Eu-CP** phosphor was successfully tested for charged fingerprints under various real-life circumstances (*e.g.*, fingers with grease, oil, sweat, and cosmetics), and on various surfaces, demonstrating its broad applicability. For practical use in unique fingerprint identification in forensic science and crime scene investigation, the phosphor powder was capable of detecting charged fingerprints with up to level-3 identifiable features (Fig. 7c).

Based on their level of detail and distinctive characteristic information, fingerprint analysis is generally divided into three different levels (levels 1–3). Each of these levels or traits helps in the identification and differentiation of individuals, even with very similar FP patterns. Level 1 traits give information on patterns of ridge lines, such as the 1st curved loops or origin, whorls, delta, and arches. The other higher-level traits are indexed and referenced by these traits. Each individual's fingerprints are developed to show a singular pattern of these characteristics and not every individual exhibits a distinct pattern of level 1 traits. Level 2 is comprised of macroscopic information such as ridges (curved lines), ridge endings, ridge bifurcations, bridges, islands, and cross-overs, known as minutiae points. The size and their distance from the core are measured and compared to identify an individual. These are ultimately used to differentiate between individuals (even twins). The microscopic level 3 features give multidimensional characteristics of ridge patterns, including incipient ridges, sweat pores, dots, and scars. These microscopic traits are highly distinct and are used in cases where level 1 and level 2 features are apparently similar for individuals; they are considered hallmarks that differentiate between fingerprints (Fig. 8a). The level 1 and level 2 features are utilized by automatic fingerprint identification systems (AFISs), which are utilized for security and forensics purposes. Nonetheless, there is a growing need for systems that can make use of level 3 characteristics for accurate LFP identification. All the level 1–3 traits were clearly visible in the fingerprint samples developed using **Eu-CP**. Thus, the **Eu-CP** can be effectively employed for the development, identification, and database management of latent fingerprints (LFP). Furthermore, the developed prints

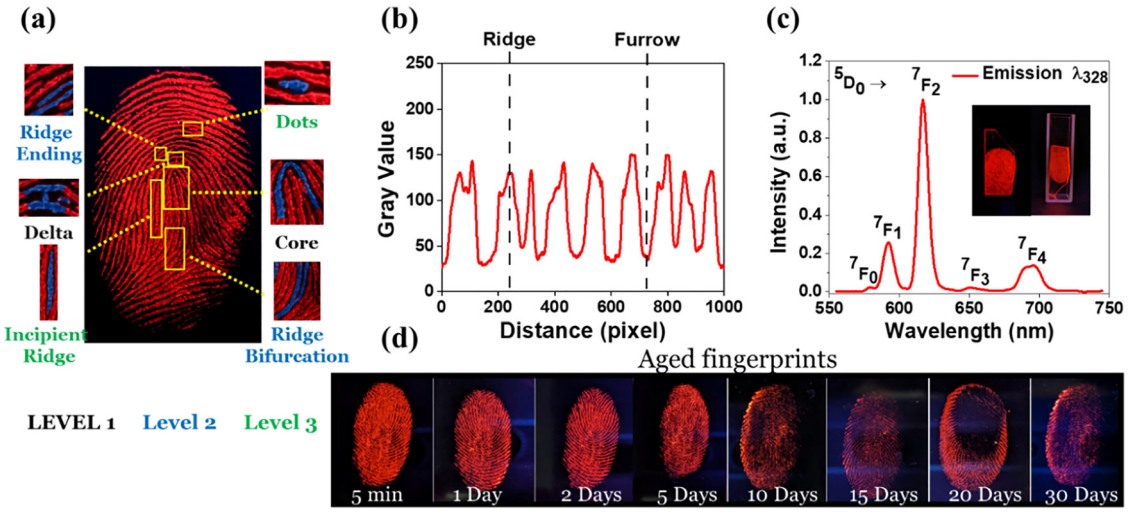

Fig. 8 (a) Determination of level 1, 2 and 3 traits in a developed fingerprint using **Eu-CP**. (b) Gray-scale plot for the image obtained after development. Sharp contrast clearly persists between the ridge and furrow, making them easily distinguishable. (c) Solid-state emission obtained by exciting **Eu-CP** developed fingerprint at 328 nm at 298 K. (d) Images of fingerprints developed using the **Eu-CP** after a defined interval on transparent glass under irradiation with a 365 nm UV light (aged test).

were assessed using International Fingerprint Research Group (IFRG) and Centre for Applied Science and Technology (CAST) scoring for desirable quality assessment of latent fingerprints.[43] We assessed the developed LFPs for the ridge area, mean fingerprint intensity, and background intensity, which were quantified using ImageJ (Fiji). High-quality fingermarks (CAST scores 2–3) were consistently observed across diverse surfaces, demonstrating the material's practical suitability for forensic fingerprint visualization (Table S2, SI). The grayscale plot for the acquired images shows a sharp contrast between the gray value of the ridge (curved lines) and furrow (interstitial space between the ridges) (Fig. 8b). This demonstrates that the bright emission from the Eu(III) center is sufficient to differentiate between the depth and curves of the developed LFPs on various surfaces. The solid-state emissions obtained using the developed fingerprint present the characteristic $^5D_0 \rightarrow {}^7F_J$ transitions of the Eu(III) (Fig. 8c). For forensic purposes, an aged sample study was conducted, and the fingerprints deposited by the donor were developed several days later (Fig. 8d). Even after 30 days, the **Eu-CP** coordination polymer retained all the trait levels and could be used to detect a fingerprint with excellent resolution.

Conclusion

In summary, this work introduces two new coordination polymers, $[Eu_2(ctpy)_6{\cdot}3H_2O]_n$ (**Eu-CP**) and $[Tb_2(ctpy)_6{\cdot}3H_2O]_n$ (**Tb-CP**) (Hctpy = 2,2′:6′,2″-terpyridine-4′-carboxylic acid), synthesized under solvothermal conditions. An array of solid- and solution-state material characterization techniques (SC-XRD, PXRD, FTIR, and NMR) was used to systematically evaluate the molecular structures of both the coordination polymers. The **Eu/Tb-CP** coordination polymers displayed characteristic red and green emissions, respectively, through energy transfer from the ctpy antenna to the emissive excited state of Eu(III)/Tb(III), which can be ascribed to the corresponding $^5D_J \rightarrow {}^7F_J$ (f–f) transitions upon excitation with UV light. The superior time-resolved luminescence property of **Eu-CP** is used for the detection of 2,4,6-tri-nitrotoluene (TNT), as a typical nitro-explosive, in the solid and solution states. The **Eu-CP** probe showed rapid, selective, and significant quenching or turn-off luminescence upon interaction with TNT compared to other studied NACs. Using different experimental techniques and observations, a probable mechanism of interaction was presented, wherein TNT molecules quench the energy transfer pathway from the ctpy antenna to Eu(III) by the PeT pathway. The interaction of **Eu-CP** and TNT was reversible due to weak non-covalent interactions; thus, the **Eu-CP**-impregnated solid strip was reused multiple times after washing away TNT with chloroform. Additionally, the strong red emissions allowed the use of **Eu-CP** as phosphor powder for the efficient, reliable, and convenient detection and development of latent fingerprints. It offers permanent and direct, colorful, high-resolution visualization with minimal background interference and allows fingerprints on various surfaces to be detected. Importantly, **Eu-CP** exhibits exceptional sensitivity and enables the detection of aged fingerprints with clear observation of level 1–3 traits, which is useful for forensic investigations. The developed phosphor powder with uniform spherical nanometer-sized particle morphology works well for the development of aged or degraded fingerprints and LFPs that are charged with greasy substances on the fingers on various surfaces without much background noise or interference. Overall, the advantageous luminescence properties of the **Eu-CP** coordination polymer were exploited in this work for the effective detection of nitro-explosives and as a very efficient and convenient method for high-resolution visualization of latent fingerprints for practical utility in forensic science. The present study underscores the utility of

responsive solid-state luminescent lanthanide materials for the detection of nitroaromatic explosives, for on-site rapid detection and development of latent fingerprints for forensic investigations, and in feasible bioauthentication-based security systems.

Experimental section

Material and methods

Lanthanide triflate salts ($La(CF_3SO_3)_3$) and furfural (2-furancarboxaldehyde) were purchased from Merck (USA). 2-Acetyl pyridine (BLD pharma, China) and $KMnO_4$ (Alfa Aesar, India) were used as received. Other reagents and solvents were obtained from Sigma Aldrich and TCI with high-grade purity (HPLC grade) and used without further purification. The reactions were carried out in standard glassware under an inert atmosphere of N_2. The solvothermal reactions were carried out in a 10 mL Teflon container enclosed in steel vessels (autoclave reactor vessels), in an AIMIL hydrothermal oven at 180 °C for 72 h. All the analytes (nitro-substituted molecules) were obtained from Sigma Aldrich, and 5 mM of each was prepared prior to the measurements. A small amount of TNT was synthesized using a simple nitration of 4-nitrotoluene and handled carefully considering its explosive nature wearing appropriate PPEs. Whatman filter paper was used for the **Eu-CP** impregnated luminescent strips. **Eu-CP** or **Tb-CP** (1.5 mg) was added to 30 mL of acetonitrile, sonicated for 30 min, and allowed to settle for 24 h before solution-state measurements. A 200 μL aliquot of supernatant was taken for each spectral measurement. The lifetime decay curves were fitted by the exponential decay method.

Titration of nitro-substituted compounds with Eu-CP

All the samples were freshly prepared in acetonitrile, sonicated, and kept undisturbed for 24 h. Before the studies, for each titration, 200 μL of supernatant was added to 1800 μL of acetonitrile. The analytes were all dissolved in acetonitrile to minimize the solvent effect and were dissolved in chloroform for the solid-state studies. All the measurements were performed in an Agilent Cary Eclipse fluorimeter. For standard measurements, a wavelength of 328 nm was used with a delay and gate time of 0.5 ms, keeping the slit widths to 5 nm each. All the measurements were performed in a quartz cuvette of 1.0 cm path length. The raw data were analyzed and plotted using Origin 9.1 software.

Latent fingerprint (LFP) detection and development

Every volunteer (n = 5) used a clean hand to deposit fingerprints on various surfaces to account for possible intra-donor variations. To account for consistency, contact time, and pressure, the latent fingerprints were taken at several times of the day and following various everyday activities. The commonly used surfaces were phones, aluminum foil, computer mice, CD-DVD, ATM cards, tabletop tiles, ceramics, tape, gloves, and glass slides. The latent fingerprint samples were aged for about 24 h prior to development, then sprinkled with finely powdered **Eu-CP** phosphors. The surface was cleaned using a fine brush, and the LFP was then placed under a UV lamp (365 nm) to reveal the latent fingerprints. The samples were next photographed using a simple smartphone camera. The photos were then converted into grayscale images using a Java-based image processing program, "ImageJ",[53] which was then also used to create grayscale value plots between the gray value and distance (pixel), which describes the luminescent contrast and quality of the fingerprint traits for reliable data. Selected fingers were charged with various substances (*e.g.* grease, hair oil, cosmetics, and sweat) and then deposited on various surfaces. The prints were then collected and processed as previously described. Surfaces used were phone, aluminum foil, plastic mouse, CD-DVD, ATM cards, tabletop tiles, ceramics, tape, gloves, and glass slides.

Instruments

^1H and ^{13}C NMR spectra (chemical shifts in δ ppm) were recorded on a JEOL JNM-ESC (400 MHz) spectrometer, using TMS as an internal standard. ESI-MS measurements were carried out using a WATERS Q-TOF Premier mass spectrometer. The UV-Vis absorption spectra were recorded on a Varian V670 UV-Vis spectrophotometer using a quartz cuvette with a path length of 1.0 cm. The time-resolved luminescence spectra were recorded using an Agilent Cary Eclipse fluorescence spectrophotometer at 298 K. The surface morphology of the **Eu-CP** was analyzed using FESEM with an accelerating voltage of 10 kV, a working distance (WD) of 7.3 mm and magnification of 50 000×. All real-time photographs were taken with a Google Pixel 7a smartphone camera under a 365 nm UV lamp. The FT-IR spectra were recorded in KBr pellets on a PerkinElmer 1320 instrument in the range 4000–400 cm^{-1}. A single crystal of suitable dimensions was mounted on a glass fiber and used for data collection. All the geometric and intensity data were collected on a Bruker D8 Quest Microfocus X-ray CCD diffractometer equipped with an Oxford Instruments low-temperature attachment, with graphite-monochromatic Mo Kα radiation (λ = 0.7103 Å) at 100(2) K using the ω-scan technique (width of 0.5° per frame) at a scan speed of 10 s per frame, controlled by the manufacturer's APEX v2012.4-3 software package.[54] Intensity data collected using the ω–2θ scan mode were corrected for Lorentz-polarization effects, processed, and integrated with Bruker's SAINT software. Absorption corrections were done using the SADABAS program.[55,56] All the crystal structures were solved in OLEX2, and models were refined by full-matrix least squares on F^2 using SHELXTL. All the non-hydrogen atoms were refined anisotropically.[57] The crystallographic diagrams and publication material were generated using OLEX2. The ORTEP view of the molecular structure and its detailed crystallographic parameters are presented.[58] The PXRD diffraction pattern of the polycrystalline material was recorded on a Rigaku Miniflex 600 two-circle diffractometer, using a Cu X-ray tube, scanning rate of 2° min^{-1} in the range 5–55° and a NaI scintillator (T1) detector. The ImageJ software was used to visualize, inspect, quantify, and validate scientific image data, and the gray-scale plot was obtained using this software. Origin Pro 2019 was used to draw the respective plots.

The lifetime measurements were performed under ambient conditions for **Eu-CP** and **Tb-CP** in H_2O and D_2O, with a pulsed Xenon lamp at λ_{ex} = 328 nm and λ_{em} = 615 nm and 545 nm, respectively, with a delay and gate time of 0.5 ms. The decay curves were fitted by the exponential decay method. The excited-state lifetime measurements in H_2O and D_2O allowed the number of water molecules (q) directly coordinated to the Eu^{3+} ion to be determined using the modified Horrocks' eqn (1).[59]

$$q = 1.1\left(\frac{1}{\tau_{H_2O}} - \frac{1}{\tau_{D_2O}} - 0.31\right) \quad (1)$$

Here, q = number of inner-sphere water molecules directly coordinated to the Eu(III) ion. τ = luminescence lifetimes of the probe in H_2O and D_2O, respectively. Limit of detection (LOD) was calculated using eqn (2):

$$\mathrm{LOD} = 3.3\sigma/s \quad (2)$$

where σ is the standard deviation of the regression line, and s is the slope of the curve obtained from the fitting of the ratio of intensity *vs.* concentration graph.

Synthesis and characterization

Synthesis of 2,2′:6′,2″-terpyridine-4′-carboxylic acid (Hctpy). Step 1: A similar method to that reported in the literature was adopted.[60a] A mixture of 2-acetylpyridine (4.49 mL, 40 mmol) and furan-2-carboxaldehyde (1.92 mg, 20 mmol) in ethanol was added with 40 mmol of KOH (230 mg). After 30 min, excess 25% ammonia solution (~60 mL), was added, and the solution was stirred for an additional 12 h. The mixture darkened and an off-white precipitate eventually formed. After 12 h, the mixture was heated at 50 °C for an hour to remove excess ammonia. The product was then filtered as an off-white solid and recrystallized in ethanol to give 2.98 g of 4 -(furan-2-yl)-2,2′:6′,2″-terpyridine **1** (f-tpy) (yield ~50%). The ^{1}H NMR data matched those of the previously reported compound so the material was used for the next step without further investigations.[60b] ^{1}H NMR (500 MHz, $CDCl_3$, 25 °C): δ 8.74 (ddd, J = 4.9, 1.9, 0.9 Hz, 2H), 8.72 (s, 2H), 8.64 (dt, J = 8.0, 1.1 Hz, 2H), 7.87 (td, J = 7.7, 1.8 Hz, 2H), 7.59 (dd, J = 1.9, 0.7 Hz, 1H), 7.38 – 7.34 (m, 2H), 7.12 (dd, J = 3.4, 0.8 Hz, 1H), 6.57 (dd, J = 3.4, 1.7 Hz, 1H) (Fig. S2, SI).

Step 2: f-tpy (0.6 g, 0.002 mol) and $KMnO_4$ (1.6 g, 0.01 mol) were added to 40 mL boiling H_2O, and the pH of the solution was adjusted to 13 using aq. 1 M NaOH solution. The mixture was then refluxed for 6 h until the complete conversion of the reactant was confirmed by TLC. The solid MnO_2 was filtered off, and the solution was neutralized with 6 M HCl and kept in a fridge at 4 °C. The off-white (yellowish) product precipitated from the reaction mixture. The solid precipitate was filtered and washed with water to give Hctpy (0.52 g, 94%). ^{1}H NMR (500 MHz, DMSO-d_6): δ 8.81 (s, 2H), 8.70 (d, J = 3.9 Hz, 2H), 8.59 (d, J = 7.9 Hz, 2H), 7.98 (td, J = 7.8, 1.7 Hz, 2H), 7.47 (dd, J = 7.4, 4.7 Hz, 2H). ^{13}C NMR (126 MHz, DMSO-d_6): δ 166.47, 154.00, 149.48, 141.47, 139.14, 127.91, 125.77, 122.01, 120.66. ESI-MS: m/z [M–H$^+$]: found, 276.0777; calcd. 276.0778. FT-IR (KBr phase, cm^{-1}): 3441(ν_{O-H}), 2927 (ν_{C-H}), 1640 ($\nu_{C=O}$) (Fig. S3, S4, SI).

Synthesis of $[Ln_2(ctpy)_6]_n$ (Ln-CP: Eu-CP, Tb-CP, La-CP). Lanthanide triflate salts (0.1 mmol) (Ln = Eu(III) and Tb(III); for **La-CP**, $LaCl_3{\cdot}6H_2O$ was used) and 0.3 mmol (84 mg) of ctpy (obtained by pretreating Hctpy with 0.31 mmol (19 mg) of NaOH taken in 4 mL H_2O) were thoroughly mixed in a Teflon beaker. The Teflon beaker was then placed in a steel vessel and heated at 180 °C for 3 days. The temperature of the oven was then reduced by 20 °C h^{-1} and the transparent crystals formed were filtered and washed with water. Suitable single crystals of **La/Eu/Tb-CPs** were mounted for data collection for structure determination using single-crystal X-ray diffraction, and the bulk polycrystalline material was characterized using PXRD.

La-CP: ^{1}H NMR (400 MHz, DMSO-d_6) δ 8.85 (s, 2H), 8.77 (dd, J = 4.9, 1.5 Hz, 2H), 8.74 (d, J = 8.0 Hz, 2H), 8.14 (td, J = 7.7, 1.6 Hz, 2H), 7.65–7.60 (m, 2H). ^{13}C NMR (101 MHz, DMSO-d_6) δ 207.09, 166.31, 155.28, 153.26, 151.35, 148.89, 146.20, 141.67, 139.92, 133.47, 126.04, 123.10, 122.47, 121.06, 31.22, 15.47. FT-IR (KBr, cm^{-1}): 3420 (ν_{O-H}), 2925 (ν_{C-H}), 1730, 1624 ($\nu_{C=O}$) (Fig. S6, S7, SI).

Conflicts of interest

The authors declare that they have no conflict of interest.

Data availability

The data supporting this article have been included as part of the SI. Synthesis and characterization of Hctpy, **Ln-CP**s, crystallographic data and tables, additional spectroscopy data, interaction of **Ln-CP**s with TNT in solution by NMR, LOD calculation, reusability of Eu-CP strips, LFP quality analysis have been included. See DOI: **https://doi.org/10.1039/d5tc02283e**.

CCDC 2380673 and 2430015 contain the supplementary crystallographic data for **Tb-CP** and **Eu-CP**, respectively for this paper.[61a,b]

Acknowledgements

We thank the Science and Engineering Research Board (SERB) for financial assistance (CRG/2021/000527) and IIT Kanpur for infrastructure. We would also like to acknowledge the Council of Scientific and Industrial Research (CSIR-09/092(1024)/2019-EMR-I), the Ministry of Human Resource and Development (MHRD), and the Prime Minister Research Fellowship-India (PMRF-PMR9042) for PhD research fellowships.

References

1 S. Cotton, *Lanthanide and actinide chemistry*, John Wiley & Sons, West Sussex, U.K., 2006.
2 J.-C. G. Bünzli, *Luminescent Probes. In Lanthanide Probes in Life, Chemical and Earth Sciences: Theory and Practice*, ed. J.-C. G. Bünzli and G. R., Amsterdam, Choppin, Elsevier, 1989.
3 K. Binnemans, *Chem. Rev.*, 2009, **109**, 4283–4374.

4 J.-C. G. Bünzli, *Chem. Lett.*, 2009, **38**, 104–109.
5 W. J. Peveler, M. Yazdani and V. M. Rotello, *ACS Sens.*, 2016, **1**, 1282–1285.
6 A. de Bettencourt-Dias, *Modern Applications of Lanthanide Luminescence*, Springer Series on Fluorescence, Springer International Publishing, Cham, Switzerland, 2023, vol. 19.
7 K. Upadhyay, S. Thomas and R. Tamraka, *Hybrid Phosphor Materials*, Springer, Cham, 2022.
8 B. Li, H.-M. Wen, Y. Cui, G. Qian and B. Chen, *Prog. Polym. Sci.*, 2015, **48**, 40–84.
9 M. Reddy, V. Divya and K. Bejoymohandas, *Dyes Pigm.*, 2023, **215**, 111248.
10 Y. Cui, B. Chen and G. Qian, *Coord. Chem. Rev.*, 2014, **273**, 76–86.
11 G. F. de Sá, O. L. Malta, C. de Mello Donegá, A. M. Simas, R. L. Longo, P. A. Santa-Cruz and E. F. da Silva, *Coord. Chem. Rev.*, 2000, **196**, 165–195.
12 S. V. Eliseeva and J.-C. G. Bünzli, *Chem. Soc. Rev.*, 2010, **39**, 189–227.
13 (*a*) K. Gupta and A. K. Patra, *ACS Sens.*, 2020, **5**, 1268–1272; (*b*) S. Pradhan, N. Shukla, G. Panigrahi and A. K. Patra, *Chem. Commun.*, 2025, **61**, 1186–1189.
14 Z. Abbas, U. Yadav, R. J. Butcher and A. K. Patra, *J. Mater. Chem. C*, 2021, **9**, 10037–10051.
15 S. W. Thomas, G. D. Joly and T. M. Swager, *Chem. Rev.*, 2007, **107**, 1339–1386.
16 S. J. Toal and W. C. Trogler, *J. Mater. Chem.*, 2006, **16**, 2871–2883.
17 X. Sun, Y. Wang and Y. Lei, *Chem. Soc. Rev.*, 2015, **44**, 8019–8061.
18 S. Khullar, S. Singh, P. Das and S. K. Mandal, *ACS Omega*, 2019, **4**, 5283–5292.
19 Y. Salinas, R. Martínez-Máñez, M. D. Marcos, F. Sancenón, A. M. Costero, M. Parra and S. Gil, *Chem. Soc. Rev.*, 2012, **41**, 1261–1296.
20 (*a*) J. H. Song and D. W. Kang, *Coord. Chem. Rev.*, 2023, **492**, 215279; (*b*) A. Dutta, A. Singh, X. Wang, A. Kumar and J. Liu, *CrystEngComm*, 2020, **22**, 7736–7781.
21 K. C. To, S. Ben-Jaber and I. P. Parkin, *ACS Nano*, 2020, **14**, 10804–10833.
22 M. J. Kangas, R. M. Burks, J. Atwater, R. M. Lukowicz, P. Williams and A. E. Holmes, *Crit. Rev. Anal. Chem.*, 2017, **47**, 138–153.
23 J. R. Askim, Z. Li, M. K. LaGasse, J. M. Rankin and K. S. Suslick, *Chem. Sci.*, 2016, **7**, 199–206.
24 M. O. Salles, G. N. Meloni, W. De Araujo and T. R. L. C. D. Paixão, *Anal. Methods*, 2014, **6**, 2047–2052.
25 N. Bolse, R. Eckstein, M. Schend, A. Habermehl, C. Eschenbaum, G. Hernandez-Sosa and U. Lemmer, *Flex. Print. Electron.*, 2017, **2**, 024001.
26 N. Bolse, R. Eckstein, A. Habermehl, G. Hernandez-Sosa, C. Eschenbaum and U. Lemmer, *ACS Omega*, 2017, **2**, 6500–6505.
27 A. Dettlaff, P. Jakóbczyk, M. Ficek, B. Wilk, M. Szala, J. Wojtas, T. Ossowski and R. Bogdanowicz, *J. Hazard. Mater.*, 2020, **387**, 121672.
28 S. J. Patil, N. Duragkar and V. R. Rao, *Sens. Actuators, B*, 2014, **192**, 444–451.
29 X. Liu, Y. Han, Y. Shu, J. Wang and H. Qiu, *J. Hazard. Mater.*, 2022, **425**, 127987.
30 X. Liu, B. Liu, G. Li and Y. Liu, *J. Mater. Chem. A*, 2018, **6**, 17177–17185.
31 H.-R. Fu, L.-B. Yan, N.-T. Wu, L.-F. Ma and S.-Q. Zang, *J. Mater. Chem. A*, 2018, **6**, 9183–9191.
32 N. Sang, C. Zhan and D. Cao, *J. Mater. Chem. A*, 2015, **3**, 92–96.
33 M. Faheem, S. Aziz, X. Jing, T. Ma, J. Du, F. Sun, Y. Tian and G. Zhu, *J. Mater. Chem. A*, 2019, **7**, 27148–27155.
34 (*a*) L. Li, J. Cheng, Z. Liu, L. Song, Y. You, X. Zhou and W. Huang, *ACS Appl. Mater. Interfaces*, 2018, **10**, 44109–44115; (*b*) B. Tan, T. H. Zhuang, E. Velasco, K. Xing, Z. F. Wu and X. Y. Huang, *Cryst. Growth Des.*, 2021, **21**, 6543–6551; (*c*) X. Zhou, H. Li, H. Xiao, L. Li, Q. Zhao, T. Yang, J. Zhu and W. Huang, *Dalton Trans.*, 2013, **42**, 5718–5723.
35 D. K. Singh, P. Majee, S. K. Mondal and P. Mahata, *Eur. J. Inorg. Chem.*, 2015, 1390–1397.
36 R. F. Bogale, Y. Chen, J. Ye, Y. Yang, A. Rauf, L. Duan, P. Tian and G. Ning, *Sens. Actuators, B*, 2017, **245**, 171–178.
37 T. S. Mahapatra, A. Dey, H. Singh, S. S. Hossain, A. K. Mandal and A. Das, *Chem. Sci.*, 2020, **11**, 1032–1042.
38 V. Jornet-Mollá, C. Dreessen and F. M. Romero, *Inorg. Chem.*, 2021, **60**, 10572–10584.
39 G. Truccolo, R. E. Boseley, S. W. Lewis and W. J. Gee, *Handbook on the physics and chemistry of rare earths*, Elsevier, 2020, vol. 57, pp. 45–117.
40 (*a*) W. Ren, G. Lin, C. Clarke, J. Zhou and D. Jin, *Adv. Mater.*, 2020, **32**, 1901430; (*b*) Z. Li, X. Liu, G. Wang, B. Li, H. Chen, H. Li and Y. Zhao, *Nat. Commun.*, 2021, **12**, 1363; (*c*) P. Li and H. Li, *Coord. Chem. Rev.*, 2021, **441**, 213988.
41 (*a*) I. M. Alaoui, Applications of luminescence to fingerprints and trace explosives detection, *Unexploded ordnance detection and mitigation*, Springer, Dordrecht, 2009; (*b*) J. Andres, R. D. Hersch, J.-E. Moser and A.-S. Chauvin, *Adv. Funct. Mater.*, 2014, **24**, 5029–5036.
42 R. Arppe and T. J. Sørensen, *Nat. Rev. Chem.*, 2017, **1**, 170031.
43 (*a*) N. Singla, M. Kaur and S. Sofat, *Forensic Sci. Int.*, 2020, **309**, 110187; (*b*) M. Wang, M. Li, A. Yu, Y. Zhu, M. Yang and C. Mao, *Adv. Funct. Mater.*, 2017, **27**, 1606243; (*c*) V. G. Sears, S. M. Bleay, H. L. Bandey and V. J. Bowman, *Sci. Justice*, 2012, **52**, 145; (*d*) J. Almog, A. A. Cantu, C. Champod and T. Kent, *J. Forensic Identif.*, 2014, **64**, 174.
44 D. Chávez, C. Garcia, J. Oliva and L. Diaz-Torres, *Ceram. Int.*, 2021, **47**, 10–41.
45 Y. Jiang, Y. Huang, X. Shi, Z. Lu, J. Ren, Z. Wang, J. Xu, Y. Fan and L. Wang, *Inorg. Chem. Front.*, 2021, **8**, 4924–4932.
46 L. Sun, Y. Zhang and X.-S. Lv, *Inorg. Chem. Commun.*, 2023, **156**, 111267.
47 Y. Shi, J. Ye, Y. Qi, M. A. Akram, A. Rauf and G. Ning, *Dalton Trans.*, 2018, **47**, 17479–17485.
48 J. Xu, T. Zhu, J. Shi, B. Song, L. Zhang, D. Zhao, X. Dong, N. Bi, J. Gou and L. Jia, *J. Rare Earths*, 2022, **40**, 1715–1727.

49 I. Olszowska-Łoś, T. Ratajczyk, I. S. Pieta, A. Siejca, J. Niedziółka-Jönsson and A. Leśniewski, *Anal. Chem.*, 2020, **92**, 15671–15678.
50 R. Fouad and M. Saif, *J. Mol. Struct.*, 2020, **1217**, 128472.
51 S. Jiang, Y.-H. Zhang, H. Wang and C.-L. Zhan, *J. Solid State Chem.*, 2020, **289**, 121481.
52 N. Li, H.-L. Guo, H.-M. Hu, J. Song, B. Xu, M.-L. Yang, F.-X. Dong and G.-L. Xue, *J. Solid State Chem.*, 2013, **198**, 416–423.
53 C. A. Schneider, W. S. Rasband and K. W. Eliceiri, *Nat. Methods*, 2012, **9**, 671–675.
54 *APEX2 v2012.4*, Bruker AXS, Madison, WI, 1999.
55 *Smart & Saint Software Reference manuals, Version 6.45*, Bruker Analytical X-ray Systems, Inc., Madison, WI, 2003.
56 G. M. S. Sheldrick, *Area Detector Absorption Correction*, University of Göttingen, Göttingen, Germany, 2001.
57 O. V. Dolomanov, L. J. Bourhis, R. J. Gildea, J. A. K. Howard and H. Puschmann, *J. Appl. Crystallogr.*, 2009, **42**, 339–341.
58 (*a*) G. M. Sheldrick, *Acta Crystallogr., Sect. A: Fundam. Crystallogr.*, 2008, **64**, 112–122; (*b*) G. M. Sheldrick, *SHELXTL 6.14, Bruker*, AXS Inc., Madison, WI, 2000.
59 W. D. Horrocks and D. R. Sudnick, *J. Am. Chem. Soc.*, 1979, **101**, 334–340.
60 (*a*) N. Shukla, V. Singhmar, J. Sayala and A. K. Patra, *Inorg. Chem.*, 2025, **64**, 1287–1301; (*b*) W. W. Fang, Z. M. Sun and T. Tu, *J. Phys. Chem. C*, 2013, **117**, 25185–25194.
61 (*a*) N. Shukla, J. Sayala, G. Panigrahi and A. K. Patra, CCDC 2380673: Experimental Crystal Structure Determination, 2025, DOI: **10.5517/ccdc.csd.cc2kx8xp**; (*b*) N. Shukla, J. Sayala, G. Panigrahi and A. K. Patra, CCDC 2430015: Experimental Crystal Structure Determination, 2025, DOI: **10.5517/ccdc.csd.cc2mkmlf**.